

ANISOTROPY STUDIES OF THE UNRESOLVED FAR-INFRARED BACKGROUND

ALEXANDRE AMBLARD, ASANTHA COORAY

Center for Cosmology, University of California, Irvine, CA 92697

Draft version January 9, 2019

ABSTRACT

Dusty, starforming galaxies and active galactic nuclei that contribute to the integrated background intensity at far-infrared wavelengths trace the large-scale structure. Below the point source detection limit, correlations in the large-scale structure lead to clustered anisotropies in the unresolved component of the far-infrared background (FIRB). The angular power spectrum of the FIRB anisotropies can be measured in surveys with the Spectral and Photometric Imaging Receiver (SPIRE) on the upcoming Herschel observatory. To study statistical properties of these anisotropies, the confusion from foreground Galactic dust emission needs to be reduced even in the “cleanest” regions of the sky. The multi-frequency coverage of SPIRE allows foreground dust to be partly separated from extragalactic anisotropies. The separation improves for fields with sizes greater than about 500 deg.² when combined with Planck data, while an area of about 1000 degrees² provides maximal information on the anisotropy power spectrum. We discuss scientific studies that can be done with anisotropy measurements of the unresolved FIRB.

Subject headings: cosmology: theory — large scale structure of universe — diffuse radiation — infrared: galaxies

1. INTRODUCTION

The total intensity of the extragalactic background light at far-IR wavelengths is now established with absolute photometry (Puget et al. 1996; Fixsen et al. 1998; Dwek et al. 1998), while deep surveys with existing or previous instruments have resolved the cosmic far-IR background (FIRB) to discreet sources at various fractions given the wavelength (see reviews in Lagache et al. 2005; Hauser & Dwek 2001). Based on these results, the FIRB light is believed to be mostly due to the thermal emission from interstellar dust in $z \sim 1$ to 3 galaxies with dust heated by ultraviolet radiation from stars and active galactic nuclei. Unfortunately, even the deepest images of far-IR sky using instruments on board the Herschel observatory¹ will be limited by source confusion. For example, at 350 μm , at most 10% of the total background intensity will be resolved to individual sources (e.g., Lagache et al. 2003). To understand properties of the sources that dominate the background light, we must study statistics of the unresolved component.

For this, a useful statistic associated with the unresolved background is the angular power spectrum of FIRB anisotropies (Haiman & Knox 2000; Knox et al. 2001; Scott & White 1999; Negrello et al. 2007). This is due to the fact that unresolved far-IR background sources are expected to trace the correlated large-scale structure and these correlations will be reflected in the unresolved fluctuations. Based on previous models, rms fluctuations are expected to be at the level of 10% of the mean intensity at sub-degree angular scales (Haiman & Knox 1999). These anisotropies can be studied with wide-field scan maps at 250 μm , 350 μm , and 500 μm from the Spectral and Photometric Imaging Receiver (SPIRE; Griffin et al. 2006) aboard Herschel. The clustering measurements can in return be used to study properties of the source distribution below the point source detection through modeling approaches such as the halo model (Cooray & Sheth 2002).

Here, we study the extent to which anisotropy measurements in the FIRB can be achieved from surveys using Herschel-SPIRE. A challenge for anisotropy measurements at these wavelengths is the confusion resulting from the thermal dust emission within our own Galaxy. We consider the extent to which the Galactic dust emission can be removed using multiwavelength information from Herschel and using Herschel complemented by Planck data. Finally, we also consider how to optimize the area of a SPIRE wide-field survey assuming a fixed observation time and consider the extent to which information related to occupation number of FIRB sources can be extracted.

The paper is organized as follows. In the next Section, we briefly discuss the angular power spectrum of far-IR anisotropies and then move on to consider removal of Galactic dust in Section 3. In Section 4 we discuss the applications of anisotropy measurements.

2. ANGULAR POWER SPECTRUM

To describe the FIRB anisotropy power spectrum, we make use of an approach based on the halo model. The angular power spectrum can be written as

$$C_\ell^{\lambda\lambda'} = \int dz \frac{dr}{dz} \frac{a^2(z)}{d_A^2} \bar{j}_\lambda(z) \bar{j}_{\lambda'}(z) P_{ss} \left(k = \frac{l}{d_A}, z \right), \quad (1)$$

where r is the conformal distance or lookback time from the observer, d_A is the comoving angular diameter distance, and $\bar{j}_\lambda(z)$ is the mean emissivity per comoving unit volume at wavelength λ as a function of redshift z for sources below a certain flux limit. Instead of intensity units, hereafter, we will work primarily in terms of antenna temperature units (μK_J) with the conversion factor for the angular power spectrum given as $\left(\frac{\partial I(\lambda)}{\partial T} \frac{\partial I(\lambda')}{\partial T} \right)^{-1} = \frac{(\lambda\lambda')^2}{4k_B^2}$. We obtain $\bar{j}_\lambda(z)$ using luminosity function models of Lagache et al. (2003). Note that the contribution to the IRB intensity, at a given wavelength, is $I_\lambda = \int_0^\infty dz \frac{dr}{dz} a(z) \bar{i}_\lambda(z)$ and can also be written as

¹<http://herschel.esac.esa.int/>

$I_\lambda = \int_0^\infty S(dN/dS)dS$ once luminosities are converted to fluxes and dN/dS is the differential number counts.

In Eq. (1), fluctuations in the source density field can be written with $P_{ss}(k) = P^{1h}(k) + P^{2h}(k)$. These two terms under the halo model are clustering of FIRB sources in two different halos (2h) and clustering within the same halo (1h):

$$\begin{aligned} P^{2h}(k) &= \left[\int dM n(M) b(M) \frac{\langle N_t(M) \rangle}{\bar{n}_g} u(k|M) \right]^2 P^{\text{lin}}(k) \\ P^{1h}(k) &= \int dM n(M) \frac{2\langle N_s \rangle \langle N_c \rangle u(k|M) + \langle N_s \rangle^2 u^2(k|M)}{\bar{n}_g^2} \end{aligned} \quad (2)$$

respectively with the halo occupation number $\langle N_t(M) \rangle = \langle N_s \rangle + \langle N_c \rangle$. Here, $u(k|M)$ is the normalized density profile in Fourier space, $n(M)$ is the halo mass function, $b(M)$ is the halo bias relative to the linear density field, and \bar{n}_g is the number densities of sources (see Cooray & Sheth 2002 for details).

In our calculations here, we make use of a simple analytical description for far-IR source occupation numbers with $\langle N_t(M, z) \rangle = 1 + \langle N_s(M) \rangle$ when $M > M_{\min}(z)$ and 0 otherwise, with the assumption of a central FIRB source in each halo ($\langle N_c(M) \rangle = 1$) above some mass scale. We take a power-law distribution of satellites with $\langle N_s(M) \rangle = A(M/M_{\min})^\beta$. We fix $A = 1$, $\beta = 0.85$ and vary M_{\min} such that we require the mean number density of galaxies, $\bar{n}_g(z) = \int dM n(M, z) \langle N_t(M, z) \rangle$, is consistent with models of luminosity functions at 350 μm from Lagache et al. (2003). This lead to M_{\min} values around 10^{12} at $z = 0$ to 10^{11} at $z \sim 3$.

At small angular scales, the finite density of sources leads to a shot-noise type power spectrum with $C_\ell^{\text{shot}} = \int_0^{S_{\text{cut}}} dS S^2 (dN/dS)$ when S_{cut} is the flux cut off value related to the removal of resolved sources. We set S_{cut} at the 5σ instrumental noise of SPIRE at each of the three bands again based on the same number count models from Lagache et al. (2003). At 250 μm , 350 μm , and 500 μm , these are 25.2, 26, 21.7 mJy for a 10 deg^2 survey integrated over 250 hours. When optimizing area at a fixed integration time, this shot-noise is varied as the survey depth is changed.

3. FOREGROUND SEPARATION

We modeled the Galactic dust with the model 8 (two temperature model) of Finkbeiner et al. (1999) and maps from Schlegel et al. (1998) (cleaned IRAS maps calibrated using DIRBE with an effective angular resolution of 6 arcminutes) over the frequency range of 217 GHz to 1200 GHz (250 μm to 1.2 mm). We increased the angular resolution up to $\ell = 10^4$ ($\simeq 1$ arcminute) by fitting the dust power spectrum at large angular scales to a power-law model. The FIRB anisotropy power spectrum modeled at 350 μm following the halo model above was interpolated to other wavelengths using the mean Fixsen et al. (1998) spectrum from COBE/FIRAS as

$$I_\nu = \tau_0 (\nu/\nu_0)^\alpha B_\nu(T), \quad (3)$$

with $\tau_0 = (1.3 \pm 0.4) \times 10^{-5}$, $T = (18.5 \pm 1.2)$ K and $\alpha = 0.64 \pm 0.12$. Using a redshift-independent SED for the frequency variation of FIRB anisotropy spectrum is only

a first approximation, since sources at different redshifts contribute to clustering at different angular scales. We tested the error resulting from this assumption using the model of Knox et al. (2001) and found the effect to be small (1%) compared to uncertainties in the mean SED.

To remove the foreground dust confusion in multiwavelength data we used the cleaning technique of Tegmark et al. (2003) by taking a linear combination of observed $a_{\ell m}$'s in each frequency band i , $a_{\ell m} = \sum_i w_i^i a_{\ell m}^i$, with weights w_i chosen to minimize foreground contamination from Galactic dust. We decompose the signal at each frequency as $a_{\ell m}^i = u_{\ell m}^i + f_{\ell m}^i + n_{\ell m}^i$ where u , f , and n stand respectively for unresolved FIRB, foregrounds (Galactic dust and CMB though CMB is not important above 500 GHz), and noise. We then minimize the resulting power spectrum of extragalactic FIRB fluctuations, assuming the frequency spectrum of this component follows that of Fixsen et al. (1998) through $\langle |a_{\ell m}|^2 \rangle = \mathbf{w}_\ell^T \mathcal{C} \mathbf{w}_\ell$ using weights under the constraint $\mathbf{w}_\ell^T \cdot \mathbf{e} = 1$, where \mathbf{e} is a column vector with the relative amplitude of the FIRB spectrum.

The above condition allows a way to optimally subtract the Galactic dust without removing the FIRB component. Here, the \mathcal{C}_ℓ^{ij} matrix represents $\langle (a_{\ell m}^i)^\dagger a_{\ell m}^j \rangle$. As derived in Tegmark et al. (2003), the weights that minimize the power $\langle |a_{\ell m}|^2 \rangle$ are

$$\mathbf{w}_\ell = \frac{\mathcal{C}^{-1} \mathbf{e}}{e^T \mathcal{C}^{-1} e}. \quad (4)$$

The estimate of residual dust level with this method is optimistic since the FIRB spectrum is poorly known. We will quantify the impact of the uncertainty related to the spectrum in terms of an overall uncertainty in the cumulative signal-to-noise ratio for detecting FIRB fluctuations in the presence of Galactic dust. To produce foreground dust spectra, we centered our simulations around commonly observed regions such as the Lockman Hole (RA,DEC = 160,56.8), XMM-LSS (RA,DEC = 33.3,-5), and CDF-S (RA,DEC = 53.6,-28) fields. To avoid contamination of FIRB fluctuations from IRAS maps (Miville-Deschénes et al. 2002), we used a minimum area of 400 deg^2 around these fields to compute the dust correlation matrix and then renormalized it using the ratio of the squared dust amplitude between smaller fields and that in the 400 deg^2 field.

In our calculations we assume an uncorrelated noise power spectrum with $\langle n_{\ell m}^i n_{\ell' m'}^j \rangle = \delta_{ij} \delta_{mm'} \delta_{\ell\ell'} N_\ell^{ii}$ between SPIRE bands. For N_ℓ' , we take 1σ noise levels for a SPIRE 10 deg^2 survey with a 250 hour integration: 1.6 mJy, 2.2 mJy, and 1.9 mJy at 250, 350, 500 μm (obtained from HSpot²) and degraded it as the survey area is increased. To combine Herschel data with Planck, we make use of 217 and 353 GHz channels of Planck HFI with equivalent noise of 13.4 and 25.2 mJy³. Since wide-field Herschel-SPIRE maps are raster-scanned, 1/f-noise impact large-scale fluctuations. We model this with $N_\ell^{ii} = N_\ell' (1 + \ell_{\text{knee}}/\ell)$ (e.g., Crawford 2007) and take $\ell_{\text{knee}} = 10^3$ corresponding to a 1/f-knee at a frequency of 100 mHz with a scan rate of 60"/sec. While we include 1/f-noise, to effectively remove it requires two passes of

²http://herschel.esac.esa.int/ao_kp_documentation.shtml

³<http://www.rssd.esa.int/Planck>

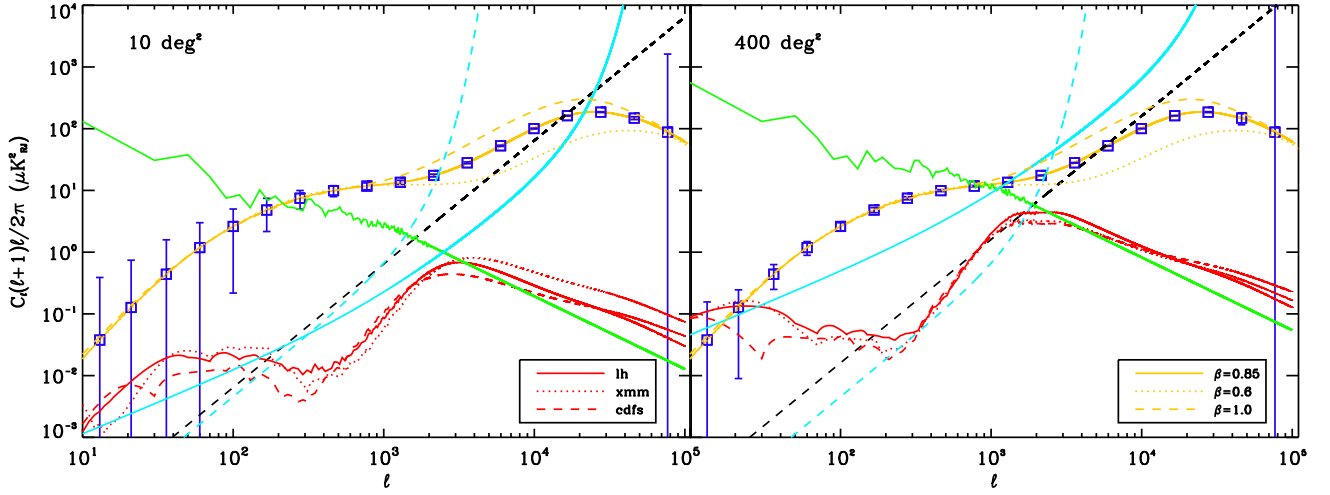


FIG. 1.— **Left:** Dust removal results for a 10 deg^2 area around the Lockman hole (lh), XMM (xmm) and CDFS (cdfs) fields. All spectra are in antenna temperature, μK_{RJ}^2 , units at $350 \mu\text{m}$. The foreground residual are the solid, dotted, dashed red lines for lh, xmm, cdfs fields. The FIRB clustering contribution is shown as orange solid, dotted, dashed lines for β of 0.85, 0.6, 1 respectively, while the Poisson term is the black dashed line. The green solid line is our model of Galactic dust power spectrum at $350 \mu\text{m}$ in the lh field. The light blue solid and dashed lines are the Herschel and Planck $350 \mu\text{m}$ detector noise. The blue squares represent the binned theoretical CIB power spectrum with its error ($\frac{\Delta\ell}{\ell} = 0.5$). **Right:** Same figure as on the left but for a 400 deg^2 area. As the shot-noise dominates clustering at smallest angular scales, we have assumed it can be removed through the amplitude of the power spectrum at $\ell > 3 \times 10^4$.

the same field in orthogonal directions. Generally, this requires that for a given area, one spend twice as long than when a survey is conducted for point source detections only. Also, given the maximum scan rate, for a fixed integration time, there is also a maximum area one can cover.

4. RESULTS & DISCUSSION

Figure 1 shows examples of the FIRB power spectrum estimated on a 10 and 400 square degree fields around the 3 fields listed above, using the 3 SPIRE bands (corresponding to central frequencies of 577, 833 and 1200 GHz) with a 250 hours integration time and 2 of Planck frequency band (217 and 353 GHz, assuming the 14 month survey). According to figure 1, both surveys can measure accurately the power spectrum of FIRB on scales smaller than 12 arcminutes ($\ell \simeq 10^3$) down to less than an arcminute when the shot-noise term begins to dominate clustering. Larger scales are not very well measured by the 10 deg^2 survey due to a large remaining cosmic variance. On the other hand, the Galactic dust residuals are much smaller for the smaller area survey at about a factor of 10 less in power.

In addition to two field sizes highlighted in Fig. 1, it could be that the angular power spectrum might be measured at a more significant level if the field size is optimized for these measurements given a finite integration time. We therefore computed the noise level and the Galactic dust level in the FIRB power spectrum estimate for different field size assuming a total of 250 hour integration time for Herschel/SPIRE observations. To show quantitatively how well different field sizes are measuring clustering of the unresolved component, we computed the total signal to noise (optimal sum on all the mode ℓ), with the sig-

nal C_{ℓ}^{clus} being the CIB power spectrum due to clustering, and the noise being the sum of the instrumental noise ($N_{\ell} = w_{\ell}^i N_{\ell}^{ii} w_{\ell}^i$) variance, the cosmic variance and the residual Galactic dust (R_{ℓ}):

$$S/N = \sqrt{\sum_{\ell=\ell_{\min}}^{\ell_{\max}} \left(\frac{C_{\ell}}{(N_{\ell} + C_{\ell}^{\text{CIB}}) \sqrt{\frac{2}{(2\ell+1)f_{\text{sky}}}} + R_{\ell}} \right)^2}, \quad (5)$$

where $C_{\ell}^{\text{CIB}} = C_{\ell} + C_{\ell}^{\text{shot}}$ and f_{sky} is the fraction of sky covered. We take $\ell_{\min} = 180/\theta$ where θ is the survey field-of-view and set $\ell_{\max} = 10^4$ so as not to be dominated by shot-noise.

The results obtained are summarized in Figure 2. The signal-to-noise ratio increases with the area covered from 50 with 3 deg^2 to 200 with 10^3 deg^2 due to the decrease of the cosmic variance, and then decreases slowly due to the increase of the Galactic dust residual. Adding the Planck channels at 217 and 353 GHz does not change much the overall sensitivity, except for very large surveys with areas greater than 400 deg^2 . Our conclusions are generally robust to an increase in the integration time, except that with an increase in the integration time, the overall signal-to-noise increases from values shown in Fig. 2 roughly by a factor $(T_{\text{int}}/250 \text{ hours})^{1/2}$.

As discussed in Section 3, to estimate the confusion associated with Galactic dust due to the uncertain extragalactic FIRB spectrum, we vary the spectrum based on uncertainties in Fixsen et al. (1998) spectrum from COBE/FIRAS by drawing 100 simulations assuming uncertainties in the parameters describing the spectrum are Gaussian distributed (see, Eq. 3). Again, we separate the Galactic dust from the FIRB and compute the total signal-to-noise ratio. Figure 2 (orange area) shows that the sen-

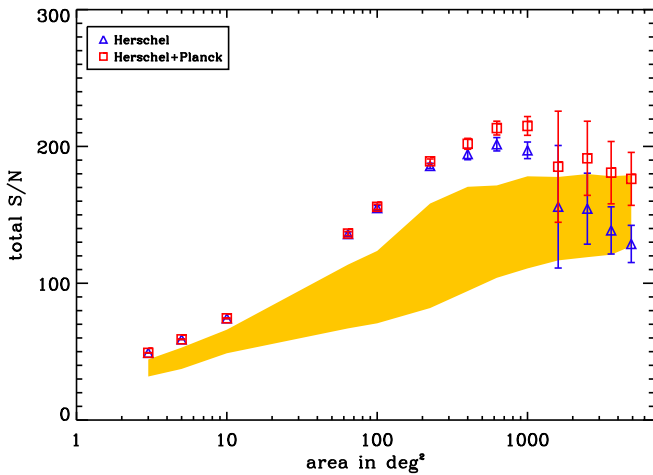


FIG. 2.— Total signal-to-noise for a detection of the FIRB power spectrum. We took into account the instrumental noise, the cosmic variance, and the foreground residuals for different sky coverage (from 3 to 5000 deg²). The blue triangles and red squares represent the average over our 3 fields (lh, cdfs, xmm) of the signal-to-noise ratio respectively with Herschel and Herschel+Planck frequencies. The error bars on the triangles and squares represent the dispersion of the signal-to-noise within the 3 fields. The solid orange area represents the signal-to-noise ratio achievable when FIRB spectrum is taken to be uncertain at the $\pm 1 \sigma$ level of Fixsen et al. (1998) analytical model (see, Eq. 3).

sitivity to the clustering is degraded by 10% to 30% on average and that the uncertainty on the FIRB spectrum generates a 15% to 30% uncertainty on the total sensitivity. Even with these uncertainties, the 1000 deg² survey remains more sensitive than the ten to a few hundred square degree survey. While uncertainties in foreground emission largely impacts the overall signal-to-noise ratio for a detection of FIRB anisotropy spectrum, an anisotropy study in a 1000 deg² field is still important given the limited knowledge we have on the unresolved component that accounts for up to 90% of the background light at 350 μ m.

To study the extent to which these anisotropy measurements can be used for astrophysical studies, we considered extraction of halo model parameters. In Figure 3, we show the expected errors on the slope parameter β on the halo occupation number and the overall bias factor describing the large angular scale clustering. To recover the occupation number in detail, clustering measurements at smaller angular scales are required to probe the 1-halo part. As shown in Fig. 1, the required measurements can be easily achieved with Herschel-SPIRE since Planck channels do not have the adequate resolution. Furthermore, the combination of Planck and Herschel over 400 deg² allows estimates of the occupation numbers and the bias factor at the level of a few percent. For larger surveys down to the same depth, there is a general improvement on parameter determination with the factor $\sqrt{f_{\text{sky}}}$.

In practice, once anisotropy measurements become available, clustering analyses can be improved by combining unresolved fluctuations with information from the clustering of resolved sources, number counts, and luminosity functions. The mechanisms to carry out such studies al-

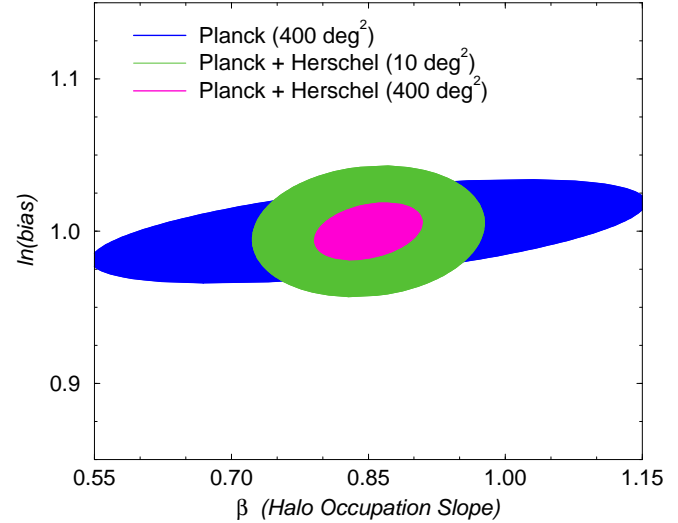


FIG. 3.— Constraints on β and the source bias factor from unresolved FIRB clustering measurements with Herschel-SPIRE and Planck.

ready exist (See example involving 3.6 μ m Spitzer data in Sullivan et al. 2007), but what is now clearly needed is a survey of required area and sensitivity. Here we have shown that a survey of order 10³ deg² provides maximal information on the clustering of unresolved fluctuations. Finally, it may also be possible to use these anisotropy maps for a weak lensing analysis in the same manner CMB maps are now proposed for lensing studies (Hu 2001). Once a better understanding 1/f-noise and scan patterns become available, it may be useful to return to such a topic.

Acknowledgments:

We thank SPIRE SAG-1 and Open-Time Key Projects groups for useful discussions and G. Lagache and J.-L. Puget for helpful suggestions. This work was supported by a McCue Fellowship (to AA).

REFERENCES

- Cooray, A. & Sheth, R. 2002, Physics Reports, 372, 1 (astro-ph/0206508)
- Crawford, T. 2007, astro-ph/0702608
- Dwek, E., et al. 1998, ApJ, 508, 106
- Griffin, M. et al. 2006, in "Studying Galaxy Evolution with Spitzer and Herschel", Crete (astro-ph/0609830)
- Hu, W. 2001, ApJ, 557, L79
- Finkbeiner, D.P., Davis, M. & Schlegel, D.J. 1999, ApJ, 524, 867
- Fixsen, D.J., Dwek, E., Mather, J.C., Bennett, C.L. & Shafer, R.A. 1998, ApJ, 508, 123
- Haiman, Z. & Knox, L. 2000, ApJ, 530, 124
- Hauser, M. & Dwek, E. 2001, ARA&A, 39, 249
- Knox, L., Cooray, A., Eisenstein, D. & Haiman, Z. 2001, ApJ, 550, 7
- Lagache, G., Dole, H. & Puget, J.-L. 2003, MNRAS, 338, 555
- Lagache, G., Puget, J.-L., Dole, H. 2005, ARA&A, 43, 727
- Miville-Deschénes, M.-A., Lagache, G., Puget, J.L. 2002, A&A, 393, 749
- Negrello, M. et al. 2007, astro-ph/0703210
- Puget, J. L. et al. 1996, A&A, 308, L5
- Schlegel, D.J., Finkbeiner, D.P. & Davis, M. 1998, ApJ, 500, 525
- Scott, D. & White, M. 1999, A&A, 346, 1
- Sullivan, I. et al. 2007, ApJ, 657, 37 (astro-ph/0609451)
- Tegmark, M., de Oliveira-Costa, A. & Hamilton, A. 2003, Phys. Rev. D, 68, 123523